Histogram analysis of intravoxel incoherent motion (IVIM)-MRI and FDG-PET parameters in breast cancer patients

Eric Edward Sigmund[1], Linda Moy[1], Jin Ah Kim[1], Sungheon Kim[1], Akshat Pujara[1], Alana Amarosa[1], Komal Jhaveri[2], James Babb[1], Christian Geppert[3], Christopher Glielmi[3], Gene Young Cho[1], Thorsten Feiweier[4], Kimberly Jackson[1], and Amy Melsaether[1]

[1]Radiology, NYU Langone Medical Center, New York, NY, United States, [2]Oncology, NYU Langone Medical Center, New York, NY, United States, [3]Siemens Medical Solutions, New York, NY, United States, [4]Healthcare Sector, Siemens AG, Erlangen, Germany

Target Audience: Physicists and radiologists interested in quantitative oncological imaging on the whole-body simultaneous MR/PET platform.

Purpose: Breast cancer imaging is increasingly incorporating a wider range of contrast mechanisms and measures of intra-tumoral heterogeneity. Diffusion-weighted imaging (DWI) and fluorodeoxyglucose (FDG) PET sense tumor cellularity and glucose consumption, respectively, and can be simultaneously measured in integrated MR/PET scanners. The intravoxel incoherent motion (IVIM) approach to DWI [1] has a growing track record in oncological imaging [2-9] for providing biomarkers of vascularity and cellularity in breast and other cancers[10-12]. Relationships between imaging biomarkers, and with individualized tumor markers, are still being explored. We compared IVIM and FDG uptake in breast cancer and studied correlations of these markers with tumor markers with histogram analysis.

Methods: A whole-body integrated 3 T MR/PET scanner (Biograph mMR, Siemens AG, Erlangen, Germany) was used to simultaneously acquire MRI and PET images of the breast in the prone position with a dedicated 4-channel breast coil using a dedicated attenuation map [13] (Noras, Würzburg, Germany) in 13 patients following their scheduled PET/CT and without additional FDG injection. Contrast-enhanced MRI was acquired with either a standard Cartesian 3D VIBE sequence or a prototype radial VIBE sequence [13]. Diffusion-weighted images were collected with a twice-refocused spin echo sequence with echo planar readout with SPAIR and extra fat suppression and inline correction of eddy-current distortions, using b-values of b= 0,30,70,100,150,200,300,400,500,800 s/mm^2. PET events were simultaneously accumulated for 15 minutes and images reconstructed on the scanner platform. DWI and histogram analysis was performed within Igor Pro (Wavemetrics, Inc.). Monoexponential decay analysis was performed using all b-values to generate apparent diffusion coefficient (ADC) maps. Regions of interest were drawn enclosing lesions on all slices on DWI with guidance both from the ADC map, post-contrast image, and PET image. All voxels within the ROIs were fitted with a voxelwise segmented algorithm to the two-compartment IVIM model to extract tissue diffusivity D_t, perfusion fraction f_p, and pseudodiffusivity D_p. Similarly, the lesions were segmented on all slices of the PET acquisition separately. Following full lesion histogram generation, mean, maximum, minimum, standard deviation, skewness and kurtosis were tabulated. Biopsy or surgical follow-up provided histological confirmation of each lesion's histological subtype, as well as expression levels of ER, PR, Ki67, and Her2/neu. Correlations were performed between imaging measures and the clinical markers.

Results: We observed 8 invasive ductal carcinomas (IDC), 2 invasive lobular carcinomas (ILC), and 3 lesions with mixed IDC/DCIS foci. Figure 1 shows an example right breast invasive ductal carcinoma (IDC) as evaluated in an MR/PET scan. Contrast-enhanced, diffusion-trace-weighted, and PET images all highlight the mass and are accurately co-registered. IVIM maps are calculated throughout the lesion, with parameter histograms shown in Figure 1. Example correlations are shown in Figure 2. The previously described inverse relationship between ADC_{min} and SUV_{max} is confirmed even in our pilot study (Fig. 2a). The heterogeneity histogram measures (standard deviation, skewness, and kurtosis) amongst biomarkers were in some cases correlated (e.g. Fig. 2b), suggesting supplemental information is carried by the IVIM/PET biomarker heterogeneity that can add to mean / extremal parameters in surrogates of tumor markers. Heterogeneity measures also showed some correlations with mean and extremal values (e.g. a direct correlation between f_p skewness and maximum SUV in Fig. 2d) suggesting that they may also be useful in conveying the scale of malignancy without complete reliance on a single maximum SUV value. Summarizing significant correlations between SUV and IVIM parameters involving the same metric (e.g. Fig. 2b) or different metrics (e.g. Fig. 2 a, d), we find 5 cross-metric f_p, 2 same-metric and 2 cross-metric ADC, and 1 cross-metric D_t correlations. We observe correlation with tumor markers, e.g. between average D_t and Her2neu (Fig. 2c) and between average D_p and ER expression (r=-0.76, p=0.027).

Discussion: The histogram analysis performed suggests correlative advantages to going beyond routine mean value sampling. The introductory parameter correlation analysis reveals statistical connections, particularly between perfusion fraction and SUV that bear further study. We postulate that the relations between blood supply (f_p), glucose consumption (SUV), and cell density (D_t) are borne out both in a voxel and in the macroscopic lesion texture, which may be capitalized upon for constructing effective surrogate clinical markers from MR/PET. This possibility can be investigated with advanced statistical, curve-fitting, texture analysis [14], or multidimensional histogram [15] tools. MR/PET is expected to amplify clinical impact of multivariate imaging, such for guidance of neoadjuvant chemotherapy.

References: 1. Le Bihan D, Radiology 1988;168(2):497-505. 2. Lemke A, Invest Radiol 2009;44(12):769-775. 3. Lu Y, J Comp Assist Tom 2013;37(3):346-352. 4. Pang Y, MRM 2012. 5. Chandarana H, Invest Radiol 2012. 6. Wang ZH, MRI 2001;19(8):1063-1072. 7. Lai V, Eur Radiol 2013;23(10):2793-2801. 8. Bisdas S, Neuroradiology 2013;55(10):1189-1196. 9. Yoon JH, JMRI 2013. 10. Sigmund EE, MRM 2011;65(5):1437-1447. 11. Liu C, Eur J Radiol 2013. 12. Kim S, Nmr in Biomedicine 2012;25(5):787-794. 13. Aklan B, Med Phys 2013;40(2):024301. 14. Ahmed A, JMRI 2013;38(1):89-101. 15. Schmidt H, Invest Radiol 2013;48(5):247-255.

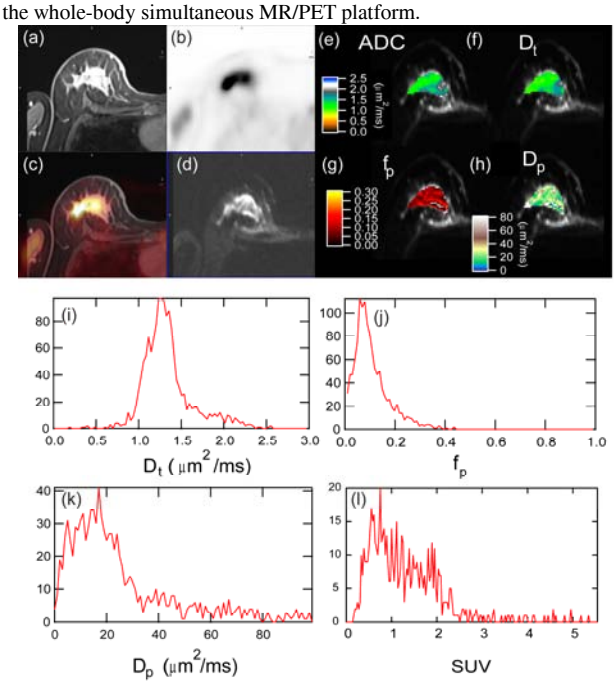

Figure 1: MR/PET images, parametric maps, and whole lesion histograms from a patient with a 4.4 cm invasive ductal carcinoma. (a) Post-contrast VIBE; (b) FDG-PET; (c) CE-MRI/PET fusion; (d) DWI b=800 s/mm^2; (e) Apparent diffusion coefficient (ADC); (f) Tissue diffusivity (D_t); (g) Perfusion fraction (f_p); (h) Pseudodiffusivity (D_p). Whole-lesion histograms of (i) D_t, (j) f_p, (k) D_p, and (l) PET standard uptake value (SUV).

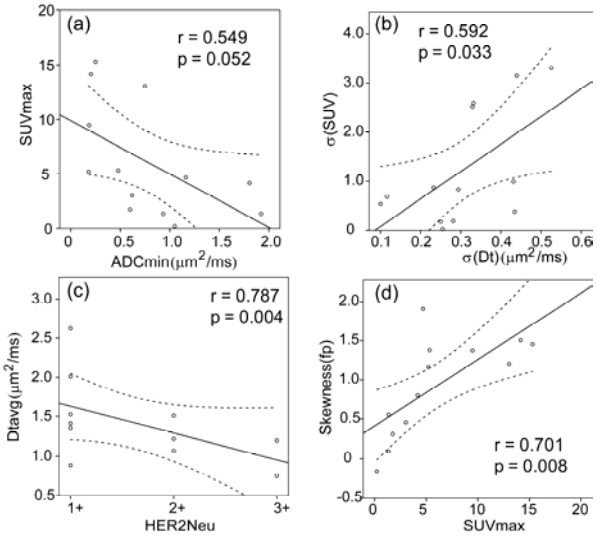

Figure 2: (a) Inverse correlation between max SUV and min ADC. (b) Correlation between standard deviations of SUV and D_t maps. (c) Inverse correlation between average D_t and Her2neu status. (d) Direct correlation between f_p skewness and max SUV. Correlations coefficients (r) and significance levels (p) are shown.